Chaos ARTICLE pubs.aip.org/aip/cha

Symmetry-protected delay spectroscopy in oscillator networks

Cite as: Chaos **36**, 073108 (2026); doi: 10.1063/5.0345354
Submitted: 26 May 2026 · Accepted: 17 June 2026 ·
Published Online: 6 July 2026

Ehsan Bolhasani,[1] Seyed Hamed Aboutalebi,[2,3,a)] and Matjaž Perc[4,5,6,7,a)]

AFFILIATIONS

[1] Department of Physics, University of Isfahan, Isfahan 81746-73441, Iran
[2] Condensed Matter National Laboratory, Institute for Research in Fundamental Sciences (IPM), Tehran 19395-5531, Iran
[3] School of Quantum Physics and Matter, Institute for Research in Fundamental Sciences (IPM), Tehran 19395-5531, Iran
[4] Faculty of Natural Sciences and Mathematics, University of Maribor, Koroška cesta 160, 2000 Maribor, Slovenia
[5] Community Healthcare Center Dr. Adolf Drolc Maribor, Ulica talcev 9, 2000 Maribor, Slovenia
[6] Department of Physics, Kyung Hee University, Dongdaemun-gu, Seoul 02447, Republic of Korea
[7] University College, Korea University, Seongbuk-gu, Seoul 02841, Republic of Korea

[a)] **Authors to whom correspondence should be addressed:** hamedaboutalebi@ipm.ir and matjaz.perc@gmail.com

ABSTRACT

We study how path-specific delays can be identified from frequency-response measurements in delay-coupled oscillator networks. Although time delays strongly shape collective dynamics, measured transfer curves usually combine many directed routes, making it difficult to determine which delayed path controls a chosen source–detector channel. We show that discrete symmetry can resolve this inverse problem. For delay-coupled Kuramoto populations on a locked Ott–Antonsen branch, a symmetry-preserving operating point enforces an exact detector–source response zero. A controlled symmetry-breaking detuning unfolds this protected zero into a ladder of real-frequency nodal crossings. We prove a general theorem for finite retarded delay networks, solve the minimal four-population motif explicitly, and show that the asymptotic spacing of the nodal ladder reads out a detector-selected delay. In the baseline motif, the recovered spacing matches the predicted delay within 0.08%, while higher-node validations recover effective delays of 2.5027 and 2.7030, in close agreement with the corresponding microscopic path delays. The result provides a swept-frequency protocol for symmetry-assisted delay spectroscopy, requiring only a selected linear detector–source response rather than reconstruction of the full transfer matrix.

Time delays are unavoidable in oscillator networks because signals need finite time to propagate, process, or interact. These delays can strongly affect synchronization, stability, and information flow, but they are difficult to infer from measurements because a single response curve usually combines many possible routes through the network. We study how symmetry can turn this problem into a path-specific measurement principle. In a delay-coupled oscillator network, a suitable symmetry can make the response between a chosen source and detector vanish exactly at a symmetric operating point. When this symmetry is then weakly broken in a controlled way, the zero response unfolds into a sequence of frequency-domain nodes. The spacing between these nodes reveals the delay of the dominant symmetry-selected path, rather than an average over the whole network. We demonstrate this mechanism for delay-coupled Kuramoto populations on a locked Ott–Antonsen branch, prove a general theorem for finite retarded delay networks, solve a minimal four-population motif, and validate the method in larger symmetric networks. The resulting protocol offers a practical form of delay spectroscopy based on swept-frequency measurements in a single selected response channel.

I. INTRODUCTION

Time delays are intrinsic to oscillator networks whenever signals require finite propagation, processing, or synaptic transmission times. In photonic and optoelectronic delay platforms, in neuronal circuits, and in broader engineered oscillator networks, these delays are not small corrections but active dynamical ingredients that can reshape collective behavior and information flow.[1–5] In delayed oscillator models, they can shift locking thresholds, stabilize or destabilize phase locking, enlarge amplitude-death regions, and reorganize modular or symmetry-related activity patterns.[6–16] Yet, this central dynamical role does not by itself make microscopic delays easy to measure.

The practical inverse problem is subtle. A measured transfer curve in a single detector–source channel typically superposes contributions from many directed routes, each carrying a phase factor $e^{-i\omega\tau}$ and each weighted by local gain and feedback. Accordingly, peaks, phase slips, and even zeros usually encode multi-path interference rather than a directly readable time of flight. Existing inference strategies address the broader problem of reconstructing interactions or causal structure from multivariate time series—via statistical similarity analysis, functional-network inference with uncertainty quantification, transfer entropy, model-free reconstruction, machine-learning link inference, or modern nonlinear causal discovery.[17–23] These approaches are powerful, but they generally target global network identification and, therefore, require richer observations than an experimentally simple channel-resolved spectroscopy. Broader network-dynamics studies, including recent work on reliability assessment in binary-state networks and simulated spreading dynamics on social networks with different topologies, further illustrate how network structure shapes dynamical observables.[24,25] These studies provide useful context for the more specific oscillator-network inverse problem addressed below.

This leads to a narrower and, for experiments, often more useful question: Given a chosen source and detector, can one identify which delayed path controls that specific response channel? Given a chosen source and detector, can one identify which delayed path controls that specific response channel? We show that discrete symmetry can make this possible. Symmetry is already known to organize collective dynamics through invariant subspaces, balanced patterns of synchrony, and cluster-synchronized states in coupled-cell and network systems.[26–29] Our use of symmetry is different. Rather than classifying which nodes synchronize together, we use it to enforce a detector–source selection rule on linear response. At a symmetry-preserving operating point, if the detector and source belong to inequivalent symmetry sectors, the corresponding scalar response vanishes identically on the real-frequency axis. A controlled one-parameter detuning then opens the forbidden inter-sector channel at first order and unfolds the protected zero into a ladder of real-frequency nodal crossings.

When a single delayed phase dominates the high-frequency symmetry-selected path expansion, the crossing locations obey

$$\omega_n = \frac{(n+\frac{1}{2})\pi - \phi}{\tau_{\text{eff}}} + O(n^{-1}), \qquad \Delta\omega_n \equiv \omega_{n+1} - \omega_n \longrightarrow \frac{\pi}{\tau_{\text{eff}}}. \tag{1.1}$$

Equation (1.1) turns a frequency sweep into a microscopic ruler. The quantity τ_{eff} is not a network average and not a black-box fit parameter; it is the delay carried by the dominant directed path that survives symmetry selection in the chosen measurement channel. Changing the detector can, therefore, select a different route and a different asymptotic spacing. The protected object in our setting is not an eigenvalue degeneracy of the delay operator but the nodal set of a scalar transfer observable, conceptually distinct from the diabolical-point framework familiar from spectral degeneracies.[30] Because the mechanism relies on a retarded linearization, each microscopic delay enters as a simple phase factor and the path interpretation remains transparent.[31]

We formulate this idea in delay-coupled Kuramoto populations with heterogeneous natural frequencies and phase-lagged sinusoidal interactions, a canonical setting for collective synchronization on networks.[32–36] For Lorentzian frequency distributions, the Ott–Antonsen reduction yields a closed macroscopic description, and with interaction delays, it retains the phase-factor structure needed for a path-based frequency-domain analysis.[37–39] Working on a locked branch serves two purposes at once: It connects the macroscopic response operator directly to a microscopic delayed ensemble, and it keeps the linearization retarded—delayed states appear, but delayed derivatives do not. This is the natural regime in which a symmetry-protected response zero can be unfolded into a measurable nodal ladder.

Recent work has further broadened the range of Kuramoto-type and related oscillator-network models in which nonpairwise interactions and additional dynamical structure shape collective behavior. Higher-order interactions can play a dual role in the stability of twisted states in high-harmonic Kuramoto–Sakaguchi models,[40] while layer-specific higher-order interactions can affect the robustness of relay synchronization in multilayer oscillator networks.[41] More generally, cooperative and competitive hyper-order interactions have been shown to reshape collective dynamics in complex networks,[42] and spatial–phase drift can modify synchronization transitions in swarmalator systems with higher-order interactions.[43] These studies emphasize how coupling architecture, interaction order, and drift-like mechanisms can reorganize synchronization dynamics. The present work is complementary: Rather than asking how these mechanisms change collective states, we use symmetry of a retarded response operator to turn a selected detector–source quadrature into a path-specific delay observable.

The present mechanism complements, but is distinct from, previous delay-based studies of functional organization in oscillator networks. Delays and frustration can reorder effective information transfer, reveal remote synchronization between symmetry-related regions, and generate functional modularity even when the structural coupling is not modular.[14–16] Our focus is more specific: We identify a detector-dependent zero-ladder observable whose asymptotic spacing isolates a path-specific microscopic delay without reconstructing the full transfer matrix. This emphasis on nodal crossings rather than resonance peaks is experimentally attractive because zeros are controlled by sign structure and phase winding, and are, therefore, less sensitive to absolute gain calibration.

In this paper, we (i) derive the locked-branch, branch-frozen response operator directly from the microscopic delayed Kuramoto ensemble; (ii) prove a general symmetry-protected ladder theorem for finite retarded delay networks; (iii) solve the minimal four-population swap motif in closed form and identify the detector-selected microscopic delay governing the baseline ladder; and (iv) validate the mechanism beyond the minimal motif and translate it into a frequency-sweep protocol. Section II derives the model and response operator. Section III introduces the minimal symmetry-protected motif. Section IV states the general theorem, and Sec. V gives the exact four-node factorization and baseline ladder law. Section VI presents validations beyond the minimal motif, while Secs. VII and VIII discuss detector specificity, delay essentiality, and the measurement protocol. Limitations are examined in Sec. IX, followed by conclusions in Sec. X. Detailed derivations, proofs, robustness analyses, and implementation details are collected in the supplementary material.

II. MODEL AND BRANCH-FROZEN RESPONSE OPERATOR

We consider a directed network partitioned into M oscillator populations. Oscillator k in population σ has phase $\theta_{\sigma,k}(t)$ and natural frequency $\omega_{\sigma,k}$, drawn from the Lorentzian density

$$g_\sigma(\omega) = \frac{\Delta_\sigma}{\pi\left[(\omega-\Omega_\sigma)^2+\Delta_\sigma^2\right]}. \tag{2.1}$$

Throughout, the first index denotes the receiver and the second the transmitter, so $K_{\sigma\eta}$ is the coupling from population η to population σ, and $\tau_{\sigma\eta}\geq 0$ is the corresponding transmission delay. The microscopic delayed Kuramoto dynamics are

$$\dot{\theta}_{\sigma,k} = \omega_{\sigma,k} + \sum_{\eta=1}^{M}\frac{K_{\sigma\eta}}{N_\eta}\sum_{j=1}^{N_\eta}\sin\left[\theta_{\eta,j}(t-\tau_{\sigma\eta})-\theta_{\sigma,k}(t)-\alpha_{\sigma\eta}\right], \tag{2.2}$$

where $\alpha_{\sigma\eta}$ is a phase lag.[32,33]

The population order parameters are

$$z_\sigma(t) = \rho_\sigma(t)e^{i\phi_\sigma(t)} = \lim_{N_\sigma\to\infty}\frac{1}{N_\sigma}\sum_{j=1}^{N_\sigma}e^{i\theta_{\sigma,j}(t)}. \tag{2.3}$$

For Lorentzian frequency distributions, the Ott–Antonsen ansatz closes the continuum dynamics on the order parameters and yields

$$\dot{z}_\sigma = -(\Delta_\sigma - i\Omega_\sigma)z_\sigma + \frac{1}{2}\sum_{\eta=1}^{M}K_{\sigma\eta}\left[e^{-i\alpha_{\sigma\eta}}z_\eta(t-\tau_{\sigma\eta}) - e^{i\alpha_{\sigma\eta}}z_\eta^*(t-\tau_{\sigma\eta})z_\sigma^2\right]. \tag{2.4}$$

This is the macroscopic delayed population model used throughout; the full continuity-equation derivation is given in the supplementary material.[37–39,44]

The spectroscopy developed below is evaluated on a locked branch of the identical-oscillator limit, $\Delta_\sigma = 0$, for which $\rho_\sigma = 1$ and

$$z_\sigma(t) = e^{i(\Omega_L t+\psi_\sigma)}. \tag{2.5}$$

Substituting Eq. (2.5) into Eq. (2.4) gives the algebraic locked-branch equations,

$$F_\sigma \equiv \Omega_\sigma - \Omega_L + \sum_{\eta=1}^{M}K_{\sigma\eta}\sin\left(\psi_\eta-\psi_\sigma-\Omega_L\tau_{\sigma\eta}-\alpha_{\sigma\eta}\right) = 0, \quad \sigma = 1,\ldots,M, \tag{2.6}$$

after fixing the gauge $\psi_1 = 0$. We allow a one-parameter family of operating points $\Omega(\delta) = \Omega^{(0)}+\delta\nu$ so that solving Eq. (2.6) defines a detuning-dependent locked branch $(\psi(\delta),\ \Omega_L(\delta))$. The symmetry-restoring value $\delta=\delta^*$ used later is specified in Sec. III; the continuation details are given in the supplementary material.

Let (ψ^*, Ω_L^*) denote a chosen operating point on the locked branch, typically δ^* or a nearby detuned state, and write

$$\phi_\sigma(t) = \Omega_L^* t + \psi_\sigma^* + x_\sigma(t), \quad |x_\sigma(t)| \ll 1. \tag{2.7}$$

With a weak external probe $u_\sigma(t)$, linearization of the phase dynamics gives

$$\dot{x}_\sigma(t) = u_\sigma(t) + \sum_{\eta=1}^{M}X_{\sigma\eta}^*\left[x_\eta(t-\tau_{\sigma\eta})-x_\sigma(t)\right], \tag{2.8}$$

where

$$\begin{aligned}\Phi_{\sigma\eta}^* &= \psi_\eta^* - \psi_\sigma^* - \Omega_L^*\tau_{\sigma\eta} - \alpha_{\sigma\eta},\\ X_{\sigma\eta}^* &= K_{\sigma\eta}\cos\Phi_{\sigma\eta}^*.\end{aligned} \tag{2.9}$$

Equation (2.8) contains delayed states but no delayed derivatives and is, therefore, a *retarded* delay equation. This distinction is essential for the high-frequency path expansion used later.[45]

For a harmonic probe $u(t) = \hat{u}\,e^{i\omega t}$ and response $x(t) = \hat{x}\,e^{i\omega t}$, Eq. (2.8) becomes

$$L(\omega;\delta)\,\hat{x} = \hat{u}, \quad H(\omega;\delta) = L(\omega;\delta)^{-1}, \tag{2.10}$$

with

$$L(\omega;\delta) = i\omega I + D_0(\delta) - X_{\rm del}^*(\omega;\delta), \tag{2.11}$$

$$[D_0(\delta)]_{\sigma\sigma} = \sum_{\eta=1}^{M}X_{\sigma\eta}^*(\delta), \tag{2.12}$$

$$[X_{\rm del}^*(\omega;\delta)]_{\sigma\eta} = X_{\sigma\eta}^*(\delta)e^{-i\omega\tau_{\sigma\eta}}.$$

Thus, every microscopic delay enters the response operator as a phase factor $e^{-i\omega\tau_{\sigma\eta}}$. The matrix $H(\omega;\delta)$ is the branch-frozen transfer operator: it maps a weak harmonic input at the selected operating point to the corresponding linear response in frequency space.

This operator is the starting point for the symmetry analysis below. Operationally, one first continues the locked branch to the desired operating point, then freezes the coefficients $X_{\sigma\eta}^*$, and finally computes the frequency response from Eq. (2.10). When the scalar detuning is differentiated, the dependence of the locked branch itself is absorbed into

$$V(\omega) = \partial_\delta L(\omega;\delta)|_{\delta=\delta^*}, \tag{2.13}$$

which is the first-order symmetry-breaking perturbation used in the nodal-ladder analysis. In the minimal motif introduced next, the detuning direction is chosen to be odd under the terminal swap, so V becomes the inter-sector bridge that unfolds the protected zero.

III. SYMMETRY-PROTECTED ZERO IN THE MINIMAL FOUR-POPULATION MOTIF

The branch-frozen response operator derived in Sec. II acquires its simplest nontrivial symmetry interpretation in a four-population directed motif with two competing delayed loops,

$$1 \to 2 \to 3 \to 1, \quad 1 \to 2 \to 4 \to 1, \tag{3.1}$$

related by the terminal swap $3 \leftrightarrow 4$. This is the minimal geometry in which a gateway detector, a symmetry-opposite source, and a symmetry-breaking detuning can coexist while preserving a microscopic delayed return path. We place the detector at node 1 and probe the motif through the antisymmetric terminal channel,

$$\begin{aligned} d &= e_1, \\ s &= e_3 - e_4, \\ G(\omega,\delta) &= d^{\dagger} H(\omega;\delta) s, \\ G(\omega,\delta) &= H_{13}(\omega;\delta) - H_{14}(\omega;\delta), \\ f(\omega,\delta) &= \operatorname{Re} G(\omega,\delta). \end{aligned} \tag{3.2}$$

Equivalently, G is the complex response at node 1 to equal-amplitude opposite-sign harmonic drives applied at the two terminal populations.

Let P_{34} denote the permutation matrix that exchanges the two terminal populations. At the symmetry-restoring operating point $\delta = \delta^*$, the locked branch and the branch-frozen coefficients are invariant under this swap, so the response operator satisfies

$$P_{34} L(\omega;\delta^*) P_{34}^{-1} = L(\omega;\delta^*), \tag{3.3}$$

$$P_{34} d = d, \quad P_{34} s = -s. \tag{3.4}$$

Hence, the resolvent $H(\omega;\delta^*) = L(\omega;\delta^*)^{-1}$ also commutes with P_{34}, and

$$G(\omega,\delta^*) = d^{\dagger} H(\omega;\delta^*) s = d^{\dagger} P_{34}^{-1} H(\omega;\delta^*) P_{34} s = -G(\omega,\delta^*). \tag{3.5}$$

Therefore,

$$G(\omega,\delta^*) \equiv 0, \quad f(\omega,\delta^*) \equiv 0 \quad \text{for all real } \omega. \tag{3.6}$$

Equation (3.6) is a protected zero line in the (ω,δ) plane, not an isolated cancellation at one tuned frequency. The mechanism is purely symmetry-based: An even detector cannot communicate with an odd source through the unperturbed symmetric resolvent.

The natural scalar detuning for this motif,

$$\Omega(\delta) = \Omega(0) + \delta\nu, \quad \nu = (0,0,1,-1)^{\mathsf{T}},$$

is odd under the same terminal swap. Moving away from δ^*, therefore, opens the forbidden detector–source channel at first order. Figure 1(a) shows the minimal four-population motif with two competing delayed loops related by the terminal swap $(3 \leftrightarrow 4)$, while Fig. 1(b) shows the contour geometry of the local unfolding of the protected zero. The entire line $\delta = \delta^*$ remains pinned at zero, while a small symmetry-breaking detuning unfolds it into transverse real-frequency crossings; near the marked point (ω_0^*, δ^*), this unfolding is locally hyperbolic. These crossings are the finite-frequency precursors of the nodal ladder analyzed in Secs. IV–IX.

This four-node motif is useful precisely because it isolates the spectroscopy mechanism in its cleanest form: Symmetry protects the baseline zero, the odd detuning opens the otherwise forbidden channel, and delayed return paths then determine the frequency spacing of the unfolded zeros. To keep the main text focused, we do not repeat the full symmetry-adapted construction here. Section S2 in the supplementary material gives the explicit even/odd decomposition, proves the decoupling of the unperturbed channels, and derives the exact first-order factorization of the unfolded response. Section IV now states the general symmetry-protected ladder theorem for finite retarded delay networks, after which Sec. V returns to the present motif to obtain the exact baseline rung law.

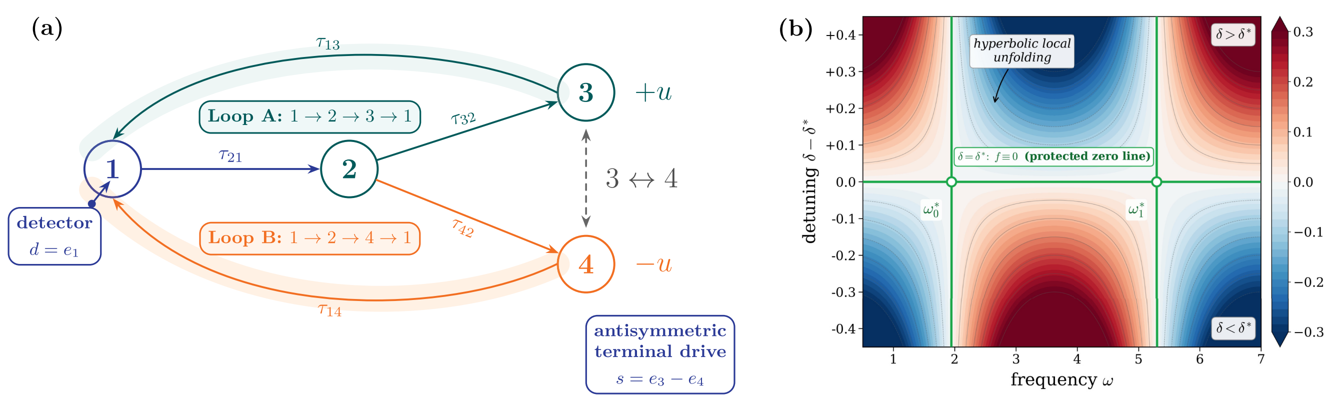

FIG. 1. Minimal four-population motif and local unfolding of the protected zero. (a) Directed four-population motif with two delayed loops, $1 \to 2 \to 3 \to 1$ and $1 \to 2 \to 4 \to 1$, related by the terminal swap $3 \leftrightarrow 4$. The selected detector is the gateway node $d = e_1$, while the selected source is the antisymmetric terminal drive $s = e_3 - e_4$, corresponding to equal-amplitude opposite-sign harmonic inputs at nodes 3 and 4. (b) Local zero-contour geometry of the scalar detector–source response $G(\omega,\delta) = d^{\dagger} H(\omega;\delta) s = H_{13}(\omega;\delta) - H_{14}(\omega;\delta)$, where $H(\omega;\delta) = L(\omega;\delta)^{-1}$ is the branch-frozen transfer matrix. The plotted real quadrature is $f(\omega,\delta) = \operatorname{Re} G(\omega,\delta) = \operatorname{Re}[H_{13}(\omega;\delta) - H_{14}(\omega;\delta)]$, shown over $\delta - \delta^* \in [-0.45, +0.45]$. The green curve marks the zero contour $f(\omega,\delta) = 0$. At the symmetry-restoring operating point $\delta = \delta^*$, the swap symmetry enforces the protected zero line $G(\omega,\delta^*) \equiv 0$ and, therefore, $f(\omega,\delta^*) \equiv 0$, for all real frequencies. A small symmetry-breaking detuning away from δ^* unfolds this protected line into transverse real-frequency nodal crossings; the local hyperbolic opening near (ω_0^*, δ^*) illustrates the first-order unfolding mechanism. This figure demonstrates the basic protected-zero/unfolding mechanism on which the delay-spectroscopy protocol is built. Parameters: $\tau_{13} = 0.90$, $\omega_0^* = 1.943$.

IV. GENERAL SYMMETRY-PROTECTED LADDER THEOREM

The four-population motif already displays the mechanism in its minimal form, but the phenomenon is not tied to that special algebra. What matters is a retarded linear response operator, a discrete symmetry that places the detector and source in inequivalent sectors, and a controlled perturbation that opens the otherwise forbidden channel. The representation-theoretic block decomposition used below is standard in symmetry-based network dynamics, and the distinction between retarded and neutral delay operators is standard in the theory of functional differential equations.[27,28,45] Here, we state only the result needed in the main text; the full projector construction, source-sector reduction, high-frequency path expansion, and proof are given in Sec. S3 in the supplementary material.

Consider a finite retarded response operator

$$L(\omega,\epsilon) = i\omega I + D_0 - \sum_{m=1}^{q} A_m e^{-i\omega\tau_m} + \epsilon V + \mathcal{O}(\epsilon^2), \tag{4.1}$$

where $\tau_m \geq 0$, the local part D_0 is evaluated at the chosen operating point, and no delayed derivatives occur. The measured observable is the scalar detector–source response

$$G(\omega,\epsilon) = \Re\left[d^\dagger L(\omega,\epsilon)^{-1} s\right], \tag{4.2}$$

with fixed detector d and source s.

The assumptions used in Theorem 1 are summarized in Table I, together with their physical roles.

Physically, A1 makes the response a sum over delayed path phases; A2 and A3 create the protected zero by placing the detector and source in inequivalent symmetry sectors; A4 supplies the controlled symmetry-breaking bridge; A5 reduces the source-sector dynamics to the channel actually probed; and A6 is the dominance condition that turns the zero sequence into a delay ruler. Thus, the assumptions are not only technical hypotheses for the theorem but also the operational conditions under which the frequency-sweep protocol identifies a detector-selected microscopic delay.

Let Π_ρ denote the isotypic projector onto sector W_ρ and define

$$\begin{aligned} H^{(0)}(\omega) &= L(\omega,0)^{-1},\\ H^{(0)}_\rho(\omega) &= \Pi_\rho H^{(0)}(\omega)\Pi_\rho,\\ V_{\alpha\beta} &= \Pi_\alpha V \Pi_\beta. \end{aligned} \tag{4.3}$$

Theorem 1 (Symmetry-protected nodal-crossing ladder): *Assume A1–A6. If $d \in W_\alpha$ and $s \in W_\beta$ with $\alpha \neq \beta$, then the unperturbed detector–source response vanishes identically on the real-frequency axis,*

$$G(\omega,0) = 0. \tag{4.4}$$

The first nonzero detuning response is

$$\partial_\epsilon G(\omega,0) = -\Re\left[d^\dagger H^{(0)}_\alpha(\omega) V_{\alpha\beta} H^{(0)}_\beta(\omega) s\right]. \tag{4.5}$$

Suppose further that the source-sector resolvent and the induced transfer amplitude satisfy

$$H^{(0)}_\beta(\omega) = \frac{u_\beta \ell_\beta^\dagger}{\Lambda_\beta(\omega)} + R_\beta(\omega), \quad \|R_\beta(\omega)\| = \mathcal{O}(|\omega|^{-2}) \tag{4.6}$$

and

$$\begin{aligned} T(\omega) = d^\dagger H^{(0)}_\alpha(\omega) V_{\alpha\beta} s_\beta &= C_*(\omega) e^{-i\omega\tau_{\rm eff}} + \sum_{p\neq *} C_p(\omega) e^{-i\omega\tau_p},\\ \eta(\omega) &:= \sum_{p\neq *}\left|\frac{C_p(\omega)}{C_*(\omega)}\right| \ll 1. \end{aligned} \tag{4.7}$$

If

$$\begin{aligned} \Lambda_\beta(\omega) &= i\omega + \mu_\beta + \mathcal{O}(1),\\ C_*(\omega) &= C_{*,\infty} + \mathcal{O}(|\omega|^{-1}), \quad C_{*,\infty}\ell_\beta^\dagger s \neq 0, \end{aligned} \tag{4.8}$$

then there exist constants $A > 0$ and $\phi \in \mathbb{R}$, such that

$$\partial_\epsilon G(\omega,0) = \frac{A}{\omega}\cos(\omega\tau_{\rm eff} + \phi) + \mathcal{O}(|\omega|^{-2}) + \mathcal{O}(\eta(\omega)). \tag{4.9}$$

TABLE I. Assumptions for Theorem 1 and their physical roles.

A1.:	$L(\omega,\epsilon)$ is a finite retarded delay operator of the form (4.1); no delayed derivatives occur. *Role:* Each microscopic delay enters as a phase factor $e^{-i\omega\tau}$, so a high-frequency delayed-path expansion is available.
A2.:	At $\epsilon = 0$, the unperturbed operator commutes with a finite-group representation $R(g)$. *Role:* The response operator decomposes into symmetry sectors at the operating point.
A3.:	The detector and source belong to inequivalent isotypic sectors: $d \in W_\alpha$, $s \in W_\beta$, $\alpha \neq \beta$. *Role:* The unperturbed detector–source response is symmetry-forbidden and, therefore, protected at zero.
A4.:	The perturbation mixes the selected sectors at first order, $\Pi_\alpha V \Pi_\beta \neq 0$, while same-sector first-order terms are absent or irrelevant for the chosen observable. *Role:* The detuning supplies the controlled symmetry-breaking bridge that opens the forbidden channel.
A5.:	In the selected source channel, the unperturbed resolvent has a rank-one dominant component $u_\beta \ell_\beta^\dagger/\Lambda_\beta(\omega)$; for multidimensional irreducible sectors, this is a statement about the multiplicity-space channel used in the measurement. *Role:* The source-sector dynamics reduce to the effective channel actually probed.
A6.:	The induced transfer amplitude has one dominant delayed phase $C_*(\omega)e^{-i\omega\tau_{\rm eff}}$ over the high-frequency tail used for zero extraction. *Role:* This dominance turns the zero sequence into a delay ruler with spacing $\pi/\tau_{\rm eff}$.

Consequently, the real zeros in the high-frequency tail satisfy

$$\omega_n = \frac{(n+\frac{1}{2})\pi - \phi}{\tau_{\rm eff}} + \mathcal{O}(n^{-1}) + \mathcal{O}(\eta),$$
$$\Delta\omega_n \equiv \omega_{n+1} - \omega_n \to \frac{\pi}{\tau_{\rm eff}}. \tag{4.10}$$

Proof sketch. At $\epsilon = 0$, Assumption A2 block-diagonalizes the unperturbed operator into isotypic sectors, so $H^{(0)}$ preserves each sector and the cross-sector response vanishes, giving Eq. (4.4). Differentiating the resolvent yields $\partial_\epsilon H|_{\epsilon=0} = -H^{(0)}VH^{(0)}$, and A4 isolates the inter-sector block opened by the perturbation. Assumption A5 reduces the selected source sector to one effective scalar denominator, while the retarded Neumann expansion of $H_\alpha^{(0)}$ writes the induced transfer amplitude $T(\omega)$ as a symmetry-filtered sum over directed delayed paths. Under A6, one delayed phase dominates that sum, so the leading term of $\partial_\epsilon G$ is the cosine in Eq. (4.9), and the zero sequence follows from the implicit-function theorem applied to its simple zeros. Section S3 in the supplementary material gives the full argument, together with the explicit high-frequency convergence bound. □

Corollary 1 (Z_2 swap case): *For a network invariant under a swap of two symmetry-related subnetworks, choose the detector in the even sector and the source in the odd sector. If the detuning is odd under the swap and mixes the two sectors at first order, then the unperturbed response is identically zero and the high-frequency rungs obey*

$$\Delta\omega_n \to \frac{\pi}{\tau_{\rm eff}} \tag{4.11}$$

whenever a single odd-to-even delayed transfer path dominates the selected tail channel.

The theorem separates symmetry selection from delay selection. Symmetry decides which detector–source channels are forbidden at the operating point; the perturbation opens the selected channel; and the dominant retarded path fixes $\tau_{\rm eff}$. Section V turns this abstract statement into an exact detector-dependent formula for the minimal four-population motif.

V. EXACT FOUR-NODE FACTORIZATION AND BASELINE LADDER LAW

We now specialize the symmetry-protected mechanism of Sec. IV to the minimal four-population motif and make the selected microscopic delay explicit. The value of the four-node problem is that the symmetry reduction is exact and the odd sector is one-dimensional, so the first-order unfolded response can be written in a closed factorized form. The detailed node-basis derivation is given in Secs. S2.8–S2.11 in the supplementary material; here, we retain only the steps needed for the main result.

For the terminal swap $3 \leftrightarrow 4$, introduce the symmetry-adapted basis

$$e_s = \frac{e_3 + e_4}{\sqrt{2}}, \quad e_a = \frac{e_3 - e_4}{\sqrt{2}} \tag{5.1}$$

and write $Q = [e_1, e_2, e_s, e_a]$. At the symmetry-restoring operating point $\delta = \delta^*$, the branch-frozen operator is block diagonal in this basis,

$$Q^T L(\omega; \delta^*) Q = L_{\rm sym}(\omega) \oplus L_{\rm anti}(\omega), \tag{5.2}$$

where $L_{\rm sym}(\omega) \in \mathbb{C}^{3\times3}$ acts on the even sector span$\{e_1, e_2, e_s\}$ and $L_{\rm anti}(\omega) \in \mathbb{C}$ acts on the odd sector span$\{e_a\}$. For the minimal motif the odd block is scalar,

$$L_{\rm anti}(\omega) = i\omega + D_s + Ye^{-i\omega\tau_{34}}. \tag{5.3}$$

This scalarization is not generic for arbitrary networks; it is the specific simplification produced here by the one-dimensional antisymmetric sector. If the terminal pair is uncoupled, then $Y = 0$ and the delayed term drops out of the odd denominator altogether.

The symmetry-breaking detuning direction $\nu = (0, 0, 1, -1)^T$ is odd under the terminal swap, so $\partial_\delta L|_{\delta^*}$ is purely off diagonal in the even/odd decomposition. Writing $\epsilon = \delta - \delta^*$ and using the resolvent identity $\partial_\delta H = -H(\partial_\delta L)H$, the protected zero unfolds as

$$f(\omega, \delta) = \epsilon g(\omega) + \mathcal{O}(\epsilon^2), \tag{5.4}$$

with

$$g(\omega) = -\sqrt{2}\,\mathrm{Re}\left[\frac{e_1^{(+)T} L_{\rm sym}(\omega)^{-1} w(\omega)}{L_{\rm anti}(\omega)}\right]. \tag{5.5}$$

Here, $e_1^{(+)} = (1, 0, 0)^T$ is the detector e_1 embedded in the even sector, and $w(\omega)$ is the effective even-sector source induced at first order by the odd detuning. Equation (5.5) is the exact first-order factorization for the four-node motif: The numerator is an even-sector transfer amplitude generated by symmetry breaking, while the denominator is the scalar odd-sector response. In the baseline branch used below, $L_{\rm anti}(\omega)$ has no real-axis zero in the scanned frequency window, so the observed rungs are zeros of the real part of Eq. (5.5), not poles or resonances.

To identify the selected delay, define the detector-dependent even-sector numerator,

$$T_d(\omega) = e_d^{(+)T} L_{\rm sym}(\omega)^{-1} w(\omega), \quad d \in \{1, 2\}, \tag{5.6}$$

where $e_1^{(+)} = (1, 0, 0)^T$ and $e_2^{(+)} = (0, 1, 0)^T$. In the high-frequency tail, the retarded path expansion gives

$$L_{\rm sym}(\omega)^{-1} = (i\omega)^{-1} I + \mathcal{O}(|\omega|^{-2}),$$
$$L_{\rm anti}(\omega)^{-1} = -\frac{i}{\omega} + \mathcal{O}(|\omega|^{-2}), \tag{5.7}$$

and the symmetry-selected numerator is dominated by one delayed transfer phase,

$$T_d(\omega) = C_{d,\infty}\, e^{-i\omega\tau_{d,\rm sel}} + \mathcal{O}(|\omega|^{-1}), \quad C_{d,\infty} \neq 0. \tag{5.8}$$

The key point is interpretive rather than algebraic: $\tau_{d,\rm sel}$ is not a network average and not a fit parameter. It is the microscopic delay carried by the dominant symmetry-selected path in the chosen detector channel.

For the baseline detector $d = e_1$, the dominant path is the closing edge from node 3 to node 1, so

$$\tau_{1,\rm sel} = \tau_{13}. \tag{5.9}$$

Moreover, in this bare-node detector channel, the leading coefficient is real up to an overall sign, so the constant phase can be absorbed

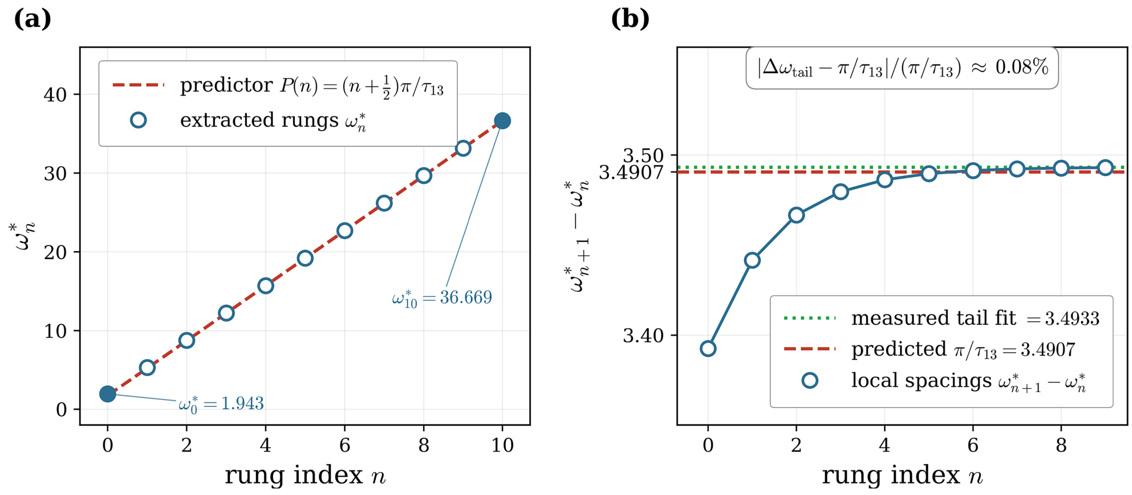

FIG. 2. Global nodal-crossing ladder and baseline spacing law for the four-node motif. (a) Extracted nodal rungs ω_n^* (open circles) for the baseline detector $d = e_1$, where each ω_n^* is a real-frequency zero of the symmetry-selected response, plotted against n, together with the asymptotic predictor $((n+\frac{1}{2})\pi)/\tau_{13}$ (dashed red line). The anchor values $\omega_0^* = 1.943$ and $\omega_{10}^* = 36.669$ are highlighted as filled squares. (b) Local spacings $\Delta\omega_n = \omega_{n+1}^* - \omega_n^*$ approach the predicted asymptotic value $\pi/\tau_{13} = 3.4907$ (dashed red line) from below. The tail-window fit, obtained from the high-frequency spacings used for delay extraction, gives 3.4933 (dashed green line), differing from the prediction by only $\sim$0.08%. The slower convergence of the first few spacings is the expected $\mathcal{O}(n^{-1})$ correction in Eq. (5.11) and does not affect the asymptotic law. These rungs are zeros of the symmetry-selected detector–source response, not resonance peaks or poles. Parameters: $\tau_{13} = 0.90$.

into the rung index. Substituting Eq. (5.8) into Eq. (5.5), therefore, yields

$$g(\omega) = \frac{A_1}{\omega}\cos(\omega\tau_{13} + \phi_1) + \mathcal{O}(|\omega|^{-2}), \quad \phi_1 = 0 \ (\mathrm{mod}\ \pi), \quad (5.10)$$

and the nodal crossings satisfy

$$\omega_n^* = \frac{\left(n+\frac{1}{2}\right)\pi - \phi_1}{\tau_{13}} + \mathcal{O}(n^{-1}), \qquad \Delta\omega_n \equiv \omega_{n+1}^* - \omega_n^* \longrightarrow \frac{\pi}{\tau_{13}}. \quad (5.11)$$

Thus, the four-node motif realizes the general theorem in its cleanest possible form: Symmetry protects the zero, the odd detuning opens the forbidden channel, and the asymptotic rung spacing reads out the selected microscopic delay τ_{13}.

Figure 2(a) is the numerical readout of Eq. (5.11) for the baseline detector $d = e_1$, displaying the agreement between the extracted nodal sequence and the asymptotic predictor

$$\frac{(n+\frac{1}{2})\pi}{\tau_{13}}.$$

The scan yields 11 positive-frequency rungs, from $\omega_0^* = 1.943$ to $\omega_{10}^* = 36.669$, and the extracted sequence follows the predictor $((n+\frac{1}{2})\pi)/\tau_{13}$ closely already at moderate rung index. The spacing plot in Fig. 2(b) is the more stringent test: The local differences converge to $\pi/\tau_{13} = 3.4907$, while the measured tail fit gives 3.4933, corresponding to a relative discrepancy of only $\sim$0.08%. The slow approach from below at small n is not a defect of the mechanism; it is precisely the subleading $\mathcal{O}(n^{-1})$ behavior allowed by Eq. (5.11).

Two points are worth emphasizing. First, the ladder in Fig. 2 is not generated by a pole of the odd-sector denominator. In the baseline window, the odd channel is regular on the real axis, so the crossings are genuine zeros of the symmetry-selected scalar response. Second, the measured spacing identifies the path delay singled out by the detector channel, here τ_{13}, rather than any average delay of the full three-edge loop. This detector dependence becomes explicit in Secs. VI–IX, where we show that changing the detector changes the selected microscopic delay and that the same symmetry logic extends beyond the minimal four-node realization.

VI. VALIDATION BEYOND THE MINIMAL MOTIF

The four-population motif establishes the mechanism in closed form, but a natural concern is whether the observed ladder is tied to the special one-dimensional odd sector of that minimal example. To test this directly, we now examine two higher-node retarded networks that realize the symmetry selection mechanism of Sec. IV in different symmetry classes. In both cases, we evaluate the signed first-order coefficient $g(\omega)$ opened by the symmetry-breaking perturbation and plot $\omega g(\omega)$, which removes the universal $1/\omega$ envelope and makes the zero sequence directly visible; the validation results are summarized in Fig. 3.

Figure 3(a) considers a six-node network with a Z_2 swap symmetry. The detector remains $d = e_1$ in the even sector, while the antisymmetric source $s = e_3 - e_4$ lies in the odd sector. The dominant symmetry-selected transfer path is $3 \to 5 \to 1$, together with its swapped partner $4 \to 6 \to 1$, so the microscopic delay singled out by the ladder law is

$$\tau_{\text{eff}} = \tau_{53} + \tau_{15} = 0.5 + 2.0 = 2.5.$$

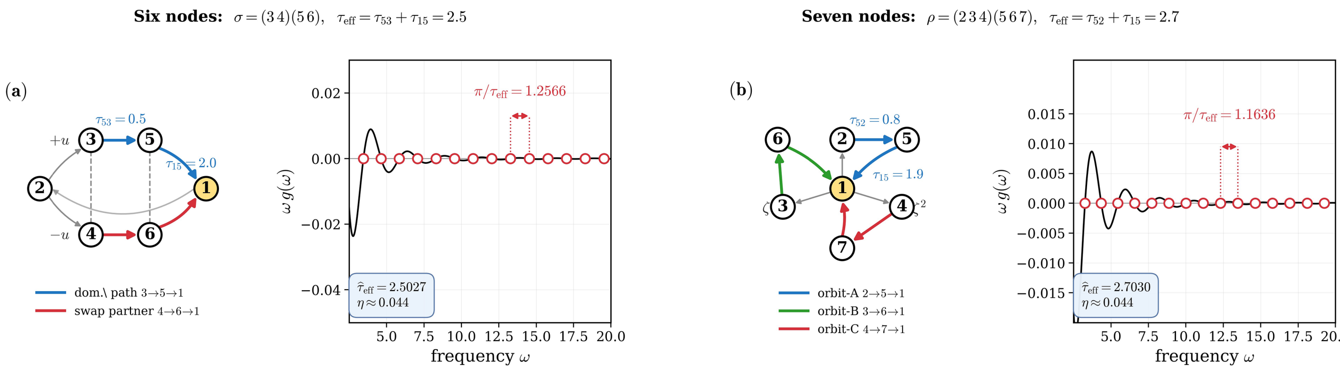

FIG. 3. Validation beyond the minimal motif. (a) Six-node swap-symmetric network with $\sigma=(3\,4)(5\,6)$. The antisymmetric source selects the odd swap sector, and the dominant symmetry-selected transfer path is $3\to5\to1$, with swap partner $4\to6\to1$. The plotted quantity is $\omega g(\omega)$, where $g(\omega)$ is the signed first-order response opened by the symmetry-breaking perturbation. Multiplication by ω removes the universal $1/\omega$ envelope and makes the asymptotic zero ladder directly visible. The selected effective delay is $\tau_{\rm eff}=\tau_{53}+\tau_{15}=0.5+2.0=2.5$, and the local spacing approaches $\pi/\tau_{\rm eff}=1.2566$. (b) Seven-node C_3-symmetric hub-and-branches network with $\rho=(2\,3\,4)(5\,6\,7)$. The dominant character-selected path is $2\to5\to1$, together with its cyclic images, giving $\tau_{\rm eff}=\tau_{52}+\tau_{15}=0.8+1.9=2.7$. Again, $\omega g(\omega)$ displays a regular zero ladder, with spacing approaching $\pi/\tau_{\rm eff}=1.1636$. These results confirm that the symmetry-protected zero-ladder mechanism persists beyond the minimal four-node motif and remains effective in higher-node networks with different symmetry classes.

The extracted crossings form a regular ladder whose local spacing tends to $\pi/\tau_{\rm eff}=1.2566$. A tail-window estimate gives $\hat\tau_{\rm eff}=2.5027$, showing that the measured spacing recovers the same path delay to within approximately 0.11%.

Figure 3(b) provides a second test in a different symmetry class. Here, the network has C_3 symmetry, the detector $d=e_1$ lies in the trivial sector, and the source is chosen in the $k=1$ character sector. The complex source used for this projection is only a convenient way to isolate a single irreducible channel; the equivalent real two-quadrature implementation is described in the supplementary material. The dominant character-selected path is $2\to5\to1$, together with its cyclic images, which gives

$$\tau_{\rm eff}=\tau_{52}+\tau_{15}=0.8+1.9=2.7.$$

The corresponding zero sequence again approaches a constant spacing, now $\pi/\tau_{\rm eff}=1.1636$. The tail-window estimate $\hat\tau_{\rm eff}=2.7030$ differs from the microscopic path delay by only approximately 0.11%.

These two examples make the main point of the section. The ladder is not an algebraic peculiarity of the exact four-node factorization of Sec. V; it persists in a larger Z_2 network and in a cyclic C_3 network, where the sector structure and dominant paths are different. In both cases, the asymptotic rung spacing again identifies the delay of a symmetry-selected directed path rather than a bulk average over all delayed edges. Full network definitions, symmetry projectors, and zero-extraction details are given in Secs. S4 and S5 in the supplementary material, and the first-order response is cross-checked against centered finite differences in Fig. S6 in the supplementary material.

VII. DETECTOR SPECIFICITY, DELAY ESSENTIALITY, AND OBSERVABLE CLASS

Intuitively, the detector is not a passive readout of a single global network delay. It projects the symmetry-unfolded response onto a particular symmetry-adapted transfer numerator. After the odd detuning opens the forbidden channel, only those delayed path contributions that have nonzero overlap with the chosen detector survive in the measured scalar quadrature. Replacing the detector, therefore, changes the projected numerator, and the leading high-frequency delayed phase can switch from one microscopic route to another. This is why $d=e_1$ selects the closing delay τ_{13} in the four-node motif, whereas $d=e_2$ selects τ_{23}.

The spectroscopy is channel-specific rather than network-wide. In the language of Secs. IV and V, changing the detector does not merely rescale the same response; it changes the symmetry-selected transfer numerator and can, therefore, change the dominant delayed path that survives in the measured channel. In the four-population motif, this is seen most clearly by replacing the gateway detector $d=e_1$ with $d=e_2$. Both detectors lie in the even swap sector, so the protected zero at $\delta=\delta^*$ survives, but the high-frequency tail is controlled by different closing delays: τ_{13} for $d=e_1$ and τ_{23} for $d=e_2$. Figure 4(a) shows the corresponding convergence of the local spacings to π/τ_{13} and π/τ_{23}. The observed change is, therefore, not a fitting artifact; it is the operational signature of detector-selected path spectroscopy.

Delay is equally essential. If all microscopic delays are rescaled uniformly, then the dominant retarded phase $e^{-i\omega\tau_{\rm eff}}$ is replaced by $e^{-i\omega\alpha\tau_{\rm eff}}$, and the nodal ladder contracts accordingly,

$$\omega_n^*(\alpha)=\alpha^{-1}\omega_n^*(1)+\mathcal{O}(n^{-1}),\quad \hat\tau_{\rm eff}(\alpha)\approx\alpha\hat\tau_{\rm eff}(1). \tag{7.1}$$

The rescaled ladders in Fig. 4(b) follow this collapse over the fitted tail window. Figure 4(c) further shows that, as α approaches zero, the number of observable rungs within a fixed frequency window decreases; accordingly, the infinite asymptotic ladder is lost in the instantaneous limit. In the instantaneous limit $\tau_{\sigma\eta}\to0$, the retarded exponential factors are removed from the resolvent, the response becomes rational in ω, and the infinite asymptotic zero ladder disappears. This provides a direct diagnostic that the measured spacing is

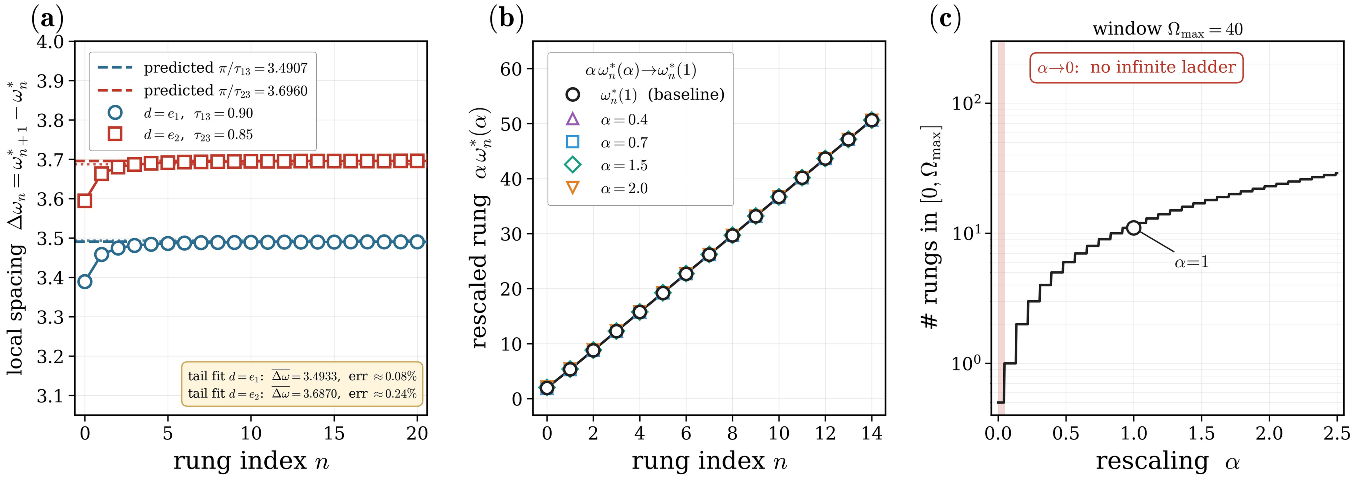

FIG. 4. Detector specificity and delay essentiality. (a) Changing the detector from e_1 to e_2 modifies the symmetry-selected transfer numerator and, therefore, selects a different microscopic delay in the four-node motif. Both e_1 and e_2 are even-sector detectors, so the protected zero at $\delta = \delta^*$ survives, but the asymptotic spacing changes from π/τ_{13} to π/τ_{23}, reflecting the detector-dependent path selection. (b) Uniform delay rescaling $\tau_{\sigma\eta} \mapsto \alpha\tau_{\sigma\eta}$ contracts the ladder according to $\omega_n^*(\alpha) \approx \alpha^{-1}\omega_n^*(1)$, confirming that the rung spacing is controlled by delay-induced phase winding. Here, $\alpha > 0$ is the rescaling factor applied to all microscopic delays. (c) Number of extracted rungs in a fixed scan window ($\Omega_{\text{scan,max}} = 40$) as a function of the rescaling factor α. As $\alpha \to 0$, corresponding to the instantaneous-delay limit, the number of observable rungs in the window decreases and the infinite asymptotic ladder disappears, demonstrating the essential role of finite delays in generating the zero ladder.

generated by delay-induced phase winding rather than by a generic oscillatory background.

Finally, the theorem is not a statement about arbitrary observables. It applies to linear detector–source responses of the form

$$G(\omega) = \mathrm{Re}\left[d^\dagger H(\omega)s\right],$$

for which detector and source can be assigned to definite symmetry sectors and the first-order perturbation opens a selected inter-sector channel. Nonlinear composites such as $|H_{13} - H_{14}|^2$, $\mathrm{Re}[H_{13}H_{24}]$, or $|H_{13}|^2$ generally mix sectors and delayed phases before the zero condition is imposed. Such observables may still exhibit isolated zeros, but those zeros are not protected by the same first-order selection rule and need not organize into a clean asymptotic ladder. For this reason, the spectroscopy protocol of Sec. VIII targets a single linear detector–source quadrature. Explicit Category-II failure templates are collected in Sec. S7 in the supplementary material, while robustness to finite population size, delay heterogeneity, observational noise, and residual symmetry breaking are summarized in Sec. S6 in the supplementary material.

VIII. FREQUENCY-SWEEP MEASUREMENT PROTOCOL

The theory above translates directly into a detector–source spectroscopy protocol that does not require reconstruction of the full transfer matrix. One fixes a symmetry-preserving locked operating point, chooses a detector d and a source s from the symmetry analysis of Secs. IV–VII, and measures only the scalar quadrature

$$\Re\left[d^\dagger H(\omega;\delta)s\right].$$

In the minimal four-population motif, this channel is

$$f(\omega,\delta) = \Re\left[H_{13}(\omega;\delta) - H_{14}(\omega;\delta)\right],$$

corresponding to the gateway detector $d = e_1$ and the antisymmetric terminal source $s = e_3 - e_4$. Experimentally, one may realize this source by applying weak opposite sinusoidal drives to the two terminal populations,

$$u_3(t) = u_0\cos(\omega t), \quad u_4(t) = -u_0\cos(\omega t), \tag{8.1}$$

with all other input components set to zero. The probe amplitude u_0 should be small enough that the response remains on the locked branch and within the linear regime of the branch-frozen description.

At the symmetry point $\delta = \delta^*$, the selected channel vanishes identically, so the useful experimental signal is the first-order unfolded response. Rather than evaluating the detuning derivative analytically, one can extract it directly from data by repeating the same frequency sweep at two nearby detunings $\delta^* + h$ and $\delta^* - h$ and forming the centered difference,

$$\widehat{g}_h(\omega) = \frac{f(\omega,\delta^*+h) - f(\omega,\delta^*-h)}{2h}. \tag{8.2}$$

For sufficiently small h, this approximates the first-order coefficient $g(\omega)$ with $O(h^2)$ error while suppressing the symmetry-protected baseline. Operationally, the protocol, therefore, requires only a weak swept-sine measurement in one detector channel, repeated at two nearby values of the scalar control parameter.

The nodal crossings are then obtained from the real zeros of $\widehat{g}_h(\omega)$. In practice, one samples $\widehat{g}_h$ on a dense frequency grid, brackets the sign changes, and refines each crossing by local interpolation or a safeguarded one-dimensional root finder. If

$$\omega_{n_0}^*, \omega_{n_0+1}^*, \ldots, \omega_{n_0+K-1}^*$$

denote a tail window of extracted rungs, the effective delay is estimated from the mean local spacing

$$\widehat{\tau}_{\text{eff}} = \frac{\pi}{\overline{\Delta\omega}}, \quad \overline{\Delta\omega} = \frac{1}{K-1}\sum_{m=0}^{K-2}\left(\omega^*_{n_0+m+1} - \omega^*_{n_0+m}\right). \tag{8.3}$$

The first few low-frequency crossings should typically be discarded because preasymptotic interference from subleading paths can distort the spacing. At the same time, frequencies that are too large are also undesirable, since the response envelope decays as $1/\omega$ and the local slope at a zero eventually approaches the experimental noise floor. The most reliable window is, therefore, the highest-frequency interval in which the crossings are still well resolved and the local spacing has already stabilized.

This protocol is detector-specific by construction. Changing the detector can select a different symmetry-adapted transfer numerator and, therefore, a different microscopic delay, as shown in Sec. VII. That dependence is not a nuisance but the central measurement principle: Detector choice acts as a selector of the delayed path whose time of flight is read from the asymptotic rung spacing. To keep the main text focused on this experimentally accessible core, the finite-difference validation of Eq. (8.2), the robustness tests against finite-N fluctuations, delay heterogeneity, and observational noise, and the complete step-by-step workflow diagram are deferred to Secs. S5–S8 and Fig. S8 in the supplementary material.

IX. DISCUSSION AND LIMITATIONS

Theoretical scope. The observable-class restriction has already been stated in Sec. VII; here, we emphasize the broader dynamical and asymptotic limits of the spectroscopy. The result proved above is a statement about a local, branch-frozen linear response measured on a symmetry-preserving locked branch. Its logic separates cleanly into three operations: symmetry protects the baseline zero, detuning opens the otherwise forbidden inter-sector channel, and retardation converts the selected microscopic delay into a frequency-domain phase winding. Accordingly, a clean asymptotic ladder should be expected only when a symmetry-preserving operating point exists, detector and source belong to inequivalent sectors, the chosen control parameter mixes those sectors at first order, and one delayed transfer phase dominates the selected high-frequency tail. If the last condition is weakened, the zero sequence need not disappear, but the local spacing can show long crossovers or beating rather than rapid convergence to a single value π/τ_{eff}.

It is useful to stress that the proposed measurement is a nodal-crossing spectroscopy, not a resonance-peak spectroscopy. The extracted delay comes from the spacing of real zeros of the first-order unfolded detector–source quadrature. These zeros are generated by the phase winding of the symmetry-selected delayed path. Resonance peaks, in contrast, are associated with gain maxima or pole proximity and can shift with damping, local amplification, and calibration. This is why the protocol uses zero locations rather than peak positions.

The theorem is also specific to retarded linearizations. This is not a technical detail. In the present setting, the linearized operator contains delayed states but no delayed derivatives, so each microscopic delay enters as a simple factor $e^{-i\omega\tau}$ and the high-frequency path expansion remains available. Neutral equations can have qualitatively different high-frequency behavior and, therefore, require a separate analysis.[45] The same caution applies to distributed-delay kernels, state-dependent delays, or parameter regimes in which several source-sector channels remain comparable: These are natural extensions of the present framework, but they are not covered by the theorem in its current form.

A second limitation is dynamical rather than algebraic. The ladder law is local to a locked branch and to the frequency window over which the branch-frozen coefficients provide an accurate description. The symmetry-protected zero at the operating point is fixed by sector selection and survives as long as the relevant symmetry is preserved, but the extracted spacing law is meaningful only while the selected locked state remains well defined. Near loss of locking, or near branch turning points and bifurcations, the usable tail window can shrink and dominant-path selection can become ambiguous. For that reason the ladder should be viewed as a diagnostic of microscopic delayed paths near a controlled operating point, not as a substitute for full nonlinear bifurcation analysis.

Experimental imperfections. Practical imperfections likewise do not invalidate the mechanism, but they set the experimental error budget. Finite population size, delay heterogeneity, observational noise, and residual symmetry breaking broaden the nodal crossings and can generate a nonzero background in the nominally protected channel. Finite-size studies of Kuramoto ensembles provide a useful baseline for how such fluctuations scale with system size.[46,47] In the present setting, they appear as uncertainty in the extracted zeros and, therefore, in $\hat{\tau}_{\text{eff}}$, while imperfect symmetry can turn exact crossings into shifted or weakly avoided ones when the residual background becomes comparable to the first-order unfolded signal. These effects are quantified for the present models in Secs. S6 and S7 and Fig. S7 in the supplementary material.

Within those limitations, the central practical message remains favorable: These limitations are not weaknesses of the method but operational conditions that indicate when the protocol should be expected to work cleanly. In that sense, the same assumptions that delimit the theorem also guide experiments by identifying the symmetry-selected detector–source channel, the controllable detuning, and the frequency window in which the nodal crossings can be resolved reliably. The protocol, therefore, still does not require reconstruction of the full transfer matrix or full network identification. Rather, it provides a practically targeted form of delay spectroscopy near a controlled operating point while also making explicit where the present theory stops.

X. CONCLUSIONS

We have shown that discrete symmetry can convert a complicated delayed transfer response into a frequency-domain ruler for a microscopic path delay. For delay-coupled Kuramoto populations on a locked Ott–Antonsen branch, a symmetry-preserving operating point produces an exactly vanishing detector–source response between inequivalent sectors. A scalar symmetry-breaking detuning then opens this forbidden channel at first order and unfolds the protected zero into a ladder of real-frequency nodal crossings whose asymptotic spacing satisfies

$$\Delta\omega_n \to \frac{\pi}{\tau_{\rm eff}}.$$

The central point is interpretive as much as it is mathematical. The quantity $\tau_{\rm eff}$ is not a bulk average and not an opaque fitting parameter. It is the delay carried by the dominant symmetry-selected directed path in the chosen detector–source channel. In the minimal four-population motif, this mechanism can be solved exactly: The unfolded response factorizes into an even-sector transfer numerator and a scalar odd-sector denominator, and the measured tail spacing recovers the selected microscopic closing delay. The same logic persists in higher-node swap-symmetric and cyclic networks, showing that the effect is not an algebraic accident of the minimal construction.

These results turn symmetry from a structural classification tool into a measurement principle. Because the protocol targets a single linear detector–source quadrature and its nodal crossings, it does not require reconstruction of the full transfer matrix or full network identification. Detector replacement selects different microscopic delays, uniform delay rescaling contracts the ladder accordingly, and the instantaneous limit removes the infinite ladder, providing direct operational checks that the measured spacing is genuinely delay-controlled.

The present theory is local to symmetry-preserving locked operating points and to retarded branch-frozen linear response. Within that scope, however, it provides a practical route to symmetry-assisted delay spectroscopy in nonlinear oscillator networks. Natural next steps are extensions to neutral or distributed-delay settings, robust automated zero extraction in noisy experimental data, and continuation of the nodal structure across branch changes and bifurcations.

SUPPLEMENTARY MATERIAL

See the supplementary material for detailed derivations of the Ott–Antonsen reduction, the four-node symmetry analysis, proofs of the general theorem, numerical validation procedures, robustness analyses, Category-II observable tests, and the frequency-sweep workflow.

ACKNOWLEDGMENTS

This work was partially supported by the Metasan (Tadbirgaran Kimia Pishtaz Co.) under Research Grant No. TKP-GRANT-M260601. The authors gratefully acknowledge this support. M.P. was supported by the Slovenian Research and Innovation Agency (Grant No. P1-0403).

AUTHOR DECLARATIONS

Conflict of Interest

The authors have no conflicts to disclose.

Author Contributions

Ehsan Bolhasani: Conceptualization (equal); Data curation (equal); Formal analysis (equal); Investigation (equal); Methodology (equal); Software (equal); Supervision (equal); Validation (equal); Visualization (equal); Writing – original draft (equal). **Seyed Hamed Aboutalebi:** Conceptualization (equal); Supervision (equal); Writing – review & editing (equal). **Matjaz Perc:** Conceptualization (equal); Supervision (equal); Writing – review & editing (equal).

DATA AVAILABILITY

The data that support the findings of this study are available from the corresponding author upon reasonable request. The custom code used for locked-branch continuation, construction of the branch-frozen response operator, resolvent evaluation, zero extraction, robustness checks, and figure generation is available from the corresponding author upon reasonable request.

REFERENCES

[1] M. C. Soriano, J. García-Ojalvo, C. R. Mirasso, and I. Fischer, Rev. Mod. Phys. **85**, 421 (2013).
[2] C. R. S. Williams, T. E. Murphy, R. Roy, F. Sorrentino, T. Dahms, and E. Schöll, Phys. Rev. Lett. **110**, 064104 (2013).
[3] B. Ermentrout and T.-W. Ko, Philos. Trans. R. Soc., A **367**, 1097 (2009).
[4] L. Larger, M. C. Soriano, D. Brunner, L. Appeltant, J. M. Gutiérrez, L. Pesquera, C. R. Mirasso, and I. Fischer, Opt. Express **20**, 3241 (2012).
[5] D. Brunner, M. C. Soriano, C. R. Mirasso, and I. Fischer, Nat. Commun. **4**, 1364 (2013).
[6] M. K. S. Yeung and S. H. Strogatz, Phys. Rev. Lett. **82**, 648 (1999).
[7] W. Gerstner, Phys. Rev. Lett. **76**, 1755 (1996).
[8] M. Dhamala, V. K. Jirsa, and M. Ding, Phys. Rev. Lett. **92**, 074104 (2004).
[9] F. M. Atay, Phys. Rev. Lett. **91**, 094101 (2003).
[10] F. M. Atay, J. Jost, and A. Wende, Phys. Rev. Lett. **92**, 144101 (2004).
[11] F. Dörfler, M. Chertkov, and F. Bullo, Proc. Natl. Acad. Sci. U.S.A. **110**, 2005 (2013).
[12] E. Oh, K. Rho, H. Hong, and B. Kahng, Phys. Rev. E **72**, 047101 (2005).
[13] A. Arenas and A. Díaz-Guilera, Eur. Phys. J.: Spec. Top. **143**, 19 (2007).
[14] V. Nicosia, M. Valencia, M. Chavez, A. Díaz-Guilera, and V. Latora, Phys. Rev. Lett. **110**, 174102 (2013).
[15] S. Khatami, E. Bolhasani, M. Perc, and A. Valizadeh, Nonlinear Dyn. **111**, 2681 (2023).
[16] E. Bolhasani, M. Hassanzadeh, M. Perc, and A. Valizadeh, Chaos, Solitons Fractals **198**, 116511 (2025).
[17] G. Tirabassi, R. Sevilla-Escoboza, J. M. Buldú, and C. Masoller, Sci. Rep. **5**, 10829 (2015).
[18] M. A. Kramer, U. T. Eden, S. S. Cash, and E. D. Kolaczyk, Phys. Rev. E **79**, 061916 (2009).
[19] R. Vicente, M. Wibral, M. Lindner, and G. Pipa, J. Comput. Neurosci. **30**, 45 (2011).
[20] O. Stetter, D. Battaglia, J. Soriano, and T. Geisel, PLoS Comput. Biol. **8**, e1002653 (2012).
[21] A. Banerjee, J. D. Hart, R. Roy, and E. Ott, Phys. Rev. X **11**, 031014 (2021).
[22] J. Runge, P. Nowack, M. Kretschmer, S. Flaxman, and D. Sejdinovic, Sci. Adv. **5**, eaau4996 (2019).
[23] J. Runge, in *Proceedings of the 36th Conference on Uncertainty in Artificial Intelligence (UAI)*, Proceedings of Machine Learning Research Vol. 124, edited by J. Peters and D. Sontag (PMLR, 2020), pp. 1388–1397.
[24] F. Wang, N. Yu, and K. Li, Chaos, Solitons Fractals **205**, 117868 (2026).
[25] K. Li, Z. Chen, R. Cong, J. Zhang, and Z. Wei, Appl. Math. Comput. **470**, 128580 (2024).
[26] I. Stewart, M. Golubitsky, and M. Pivato, SIAM J. Appl. Dyn. Syst. **2**, 609 (2003).

[27] L. M. Pecora, F. Sorrentino, A. M. Hagerstrom, T. E. Murphy, and R. Roy, Nat. Commun. **5**, 4079 (2014).
[28] F. Sorrentino, L. M. Pecora, A. M. Hagerstrom, T. E. Murphy, and R. Roy, Sci. Adv. **2**, e1501737 (2016).
[29] F. Della Rossa, L. Pecora, K. Blaha, A. Shirin, I. Klickstein, and F. Sorrentino, Symmetries and cluster synchronization in multilayer networksNat. Commun. **11**, 3179 (2020).
[30] M. V. Berry and M. Wilkinson, Proc. R. Soc. A **392**, 15 (1984).
[31] W. Michiels and S.-I. Niculescu, *Stability and Stabilization of Time-Delay Systems: An Eigenvalue-Based Approach* (SIAM, Philadelphia, PA, 2007).
[32] Y. Kuramoto, in *International Symposium on Mathematical Problems in Theoretical Physics*, Lecture Notes in Physics Vol. 39, edited by H. Araki (Springer, Berlin, Heidelberg, 1975), pp. 420–422.
[33] J. A. Acebrón, L. L. Bonilla, C. J. Pérez Vicente, F. Ritort, and R. Spigler, Rev. Mod. Phys. **77**, 137 (2005).
[34] S. H. Strogatz, Physica D **143**, 1 (2000).
[35] A. Pikovsky, M. Rosenblum, and J. Kurths, *Synchronization: A Universal Concept in Nonlinear Sciences* (Cambridge University Press, Cambridge, 2001).
[36] A. Arenas, A. Díaz-Guilera, J. Kurths, Y. Moreno, and C. Zhou, Phys. Rep. **469**, 93 (2008).
[37] E. Ott and T. M. Antonsen, Chaos **18**, 037113 (2008).
[38] E. Ott and T. M. Antonsen, Chaos **19**, 023117 (2009).
[39] W. S. Lee, E. Ott, and T. M. Antonsen, Phys. Rev. Lett. **103**, 044101 (2009).
[40] X. Wang, D. Yu, Y. Xie, X. Li, Z. Ye, and Y. Jia, Chaos, Solitons Fractals **208**, 118263 (2026).
[41] X. Hu, Q. Ding, Y. Xie, Z. Ye, and Y. Jia, Chaos, Solitons Fractals **209**, 118541 (2026).
[42] Y.-p. Hu, D. Yu, X.-q. Wang, T.-y. Li, X.-n. Li, and Y. Jia, Phys. Rev. E **113**, 054308 (2026).
[43] Y. Hu, D. Yu, T. Li, Y. Wu, Q. Ding, and Y. Jia, Commun. Phys. **8**, 177 (2025).
[44] B. Pietras and A. Daffertshofer, Chaos **26**, 103101 (2016).
[45] J. K. Hale and S. M. Verduyn Lunel, *Introduction to Functional Differential Equations* (Springer, New York, 1993).
[46] T. Coletta, R. Delabays, and P. Jacquod, Phys. Rev. E **95**, 042207 (2017).
[47] S.-C. Park and H. Park, Phys. Rev. E **110**, 034216 (2024).